2014

Lateral-Mode Vibration of Microcantilever-Based Sensors in Viscous Fluids Using Timoshenko Beam Theory

Joshua Schultz
Milwaukee School of Engineering

Stephen M. Heinrich
Marquette University, stephen.heinrich@marquette.edu

Fabien Josse
Marquette University, fabien.josse@marquette.edu

Isabelle Dufour
Université de Bordeaux

Nicholas J. Nigro
Marquette University, nicholas.nigro@marquette.edu

See next page for additional authors

Lateral-Mode Vibration of Microcantilever-Based Sensors in Viscous Fluids Using Timoshenko Beam Theory*

Joshua A. Schultz, [1,2] Stephen M. Heinrich,[1] Fabien Josse, [3] Isabelle Dufour,[4] Nicholas J. Nigro,[5] Luke A. Beardslee,[6] Oliver Brand [6]

[1]Department of Civil, Construction and Environmental Engineering, Marquette University, Milwaukee, WI, USA

[2]Milwaukee School of Engineering, Milwaukee, WI, USA (current affiliation)

[3]Department of Electrical and Computer Engineering, Marquette University, Milwaukee, WI, USA

[4]Université de Bordeaux, CNRS, IMS Laboratory, Talence, France

[5]Department of Mechanical Engineering, Marquette University, Milwaukee, WI, USA

[6]School of Electrical and Computer Engineering, Georgia Institute of Technology, Atlanta, USA

*The citation for the published version of this manuscript is the following:

Schultz, J.A., Heinrich, S.M., Josse, F., Dufour, I., Nigro, N.J., Beardslee, L.A., and Brand, O., "Lateral-Mode Vibration of Microcantilever-based Sensors in Viscous Fluids Using Timoshenko Beam Theory," **Journal of Microelectromechanical Systems,** DOI:10.1109/JMEMS.2014.2354596, available online Sept. 2014, 13 pp.

ABSTRACT

To more accurately model microcantilever resonant behavior in liquids and to improve lateral-mode sensor performance, a new model is developed to incorporate viscous fluid effects and "Timoshenko beam" effects (shear deformation, rotatory inertia). The model is motivated by studies showing that the most promising geometries for lateral-mode sensing are those for which Timoshenko effects are most pronounced. Analytical solutions for beam response due to harmonic tip force and electrothermal loadings are expressed in terms of total and bending displacements, which correspond to laser and piezoresistive readouts, respectively. The influence of shear deformation, rotatory inertia, fluid properties, and actuation/detection schemes on resonant frequencies (f_{res}) and quality factors (Q) are examined, showing that Timoshenko beam effects may reduce f_{res} and Q by up to 40% and 23%, respectively, but are negligible for width-to-length ratios of 1/10 and lower. Comparisons with measurements (in water) indicate that the model predicts the qualitative data trends but underestimates the softening that occurs in stiffer specimens, indicating that support deformation becomes a factor. For thinner specimens the model estimates Q quite well, but exceeds the observed values for thicker specimens, showing that the Stokes resistance model employed should be extended to include pressure effects for these geometries.

Keywords/index terms -- microcantilevers, resonant frequency, quality factor, liquid-phase sensing, lateral mode, vibrations.

I. INTRODUCTION

Chemical and biochemical sensing is an active and rapidly developing field, resulting in an ever-increasing presence of micro/nanoelectromechanical systems (MEMS/NEMS) in a variety of diagnostic, monitoring, and security applications. However, many of these applications necessitate liquid-phase sensing, which poses significant challenges for dynamic-mode sensors due to the drastic reduction in resonant frequency (f_{res}) and quality factor (Q) that occurs due to the liquid [1-4]. To overcome such challenges, recent research has focused on the use of (a) alternative vibrational modes of microcantilevers in lieu of the fundamental transverse flexural mode or (b) efficient modes in structures of non-cantilever geometry. The former category includes investigations of higher modes of transverse flexure [2, 5-8], longitudinal modes [9-11], torsional modes [2, 6, 8, 12-15], and lateral (in-plane) flexural modes [10, 13, 16-22]. Recent studies on novel, non-cantilever designs that reduce fluid resistance via in-plane oscillations include a bridge beam supporting two half-disks [23] and a microstructure comprising a rotating disk supported and driven by two tangentially oriented legs [24-28]. All of these studies were primarily motivated by the desire to reduce the detrimental effects of fluid damping and fluid inertia, thus providing higher resonant frequencies, f_{res} , and quality factors, Q , the latter corresponding to sharper resonant peaks. Within the context of sensing applications, such improvements in the resonant characteristics correspond to enhancements in sensor performance metrics such as mass or chemical sensitivity and limit of detection, especially for liquid-phase detection (e.g., [20, 29-31]).

Several of the aforementioned studies on the use of the lateral flexural mode in microcantilevers in liquids demonstrated both theoretically [17-18, 22] and

experimentally [19, 21] that the improvements in the in-liquid resonant characteristics will be most pronounced in microbeams that are relatively short and wide. However, the conclusions in the theoretical studies were based on Euler-Bernoulli beam theory whose accuracy is known to deteriorate for short, wide beams deforming in the lateral mode. This loss of accuracy in the Euler-Bernoulli theory and a likely reason for the departure of Euler-Bernoulli theoretical results from the measured f_{res} and Q data in liquids are the effects of shear deformation and rotatory inertia, neglected in Euler-Bernoulli theory, which become increasingly important in shorter, wider microcantilevers [21]. Because these are precisely the geometries that show the most promise in lateral-mode liquid-phase sensing applications, a strong motivation clearly exists to generalize the previous Euler-Bernoulli modeling efforts to account for transverse shear strain as well as the mass associated with the rotation of beam cross sections, i.e., the so-called Timoshenko beam effects. Hence, the aim of the present study is to derive and evaluate a Timoshenko beam model for a laterally vibrating microcantilever in the presence of a viscous fluid, as the predicted resonant behavior of such a system is of direct relevance to the performance of lateral-mode sensing devices.

While there exist a few attempts to utilize Timoshenko beam models in MEMS/NEMS applications, their focus has tended to be on the transverse flexural mode and atomic force microscopy (AFM) applications [32-35] or on the influence of surface effects [36-37]. Moreover, with the exception of one reference [34], none of these models incorporates the effects of a surrounding fluid. The objective of the investigation in [34] was to study the influence of fluid damping on the frequency response of (transverse-mode) AFM cantilevers; however, the damping coefficients employed in that

study were not related to the fundamental properties of the surrounding fluid, nor was the fluid's contribution to the system's effective mass included. In short, none of the existing Timoshenko beam models is relevant to lateral-mode, liquid-phase, microcantilever-based sensing, the application of interest in the present study.

II. PROBLEM STATEMENT

Consider a microcantilever beam immersed in a viscous fluid which experiences a flexural vibration along the y-direction of Fig. 1. The effects of shear deformation and rotatory inertia in the beam ("Timoshenko beam effects") are to be included, as are the inertial and damping effects of the surrounding fluid. The relevant geometric and material parameters of the system are specified in Fig. 1, while the loading parameters for the two load cases of interest are indicated in Fig. 2. The geometric parameters include the length (L), width (b), and thickness (h) of the cantilever. Because the microcantilever thickness is typically small relative to the width, the flexural vibrations along the y-direction are termed "in-plane" or "lateral." Material properties for the beam include its mass density (ρ_b), Young's modulus (E), and shear modulus (G). (When applied to an anisotropic material such as silicon, the latter two properties correspond to the longitudinal (x) and in-plane (x-y) directions, respectively.) The fluid is characterized by its mass density (ρ_f) and dynamic viscosity (η).

Two particular forms of in-plane loading are considered (Fig. 2): Load Case I involves a harmonically varying imposed rotation at the supported end, with amplitude θ_0 and (circular) frequency ω. In Load Case II the beam is excited by a harmonically varying tip force of amplitude F_0 and frequency ω. These two load cases are considered because they represent two of the more common excitation types used in microcantilever-

based sensing applications. For example, Load Case I simulates an electrothermal excitation scheme that has been successfully implemented recently for lateral-mode sensing applications (e.g., [19]). That method, which involves imposing longitudinal thermal strains at the extreme fibers near the support, may be represented kinematically as an imposed harmonic rotation at the support [18], thus providing the motivation for Load Case I. The second loading case is chosen because a tip force loading may be induced when electromagnetic actuation methods are used in dynamic-mode sensing applications. For each of the two load cases, we wish to formulate and solve the boundary value problem (BVP) that governs the in-plane vibration of the Timoshenko cantilever beam in fluid.

Our focus shall be on determining two particular response histories: (1) the total displacement at the beam tip, $v(L,t)$, and (2) the bending-deformation displacement, $v_{B-D}(L,t)$, at the beam tip, i.e., that portion of the total tip displacement that is due to bending deformation *only* (not due to shear deformation or, for Load Case I, rigid body rotation). The total displacement at the tip is the relevant response quantity for sensor applications that utilize optical (laser) monitoring of the tip position, while the tip's bending-deformation displacement at or near resonance will be approximately proportional to the beam's bending strain, i.e., it will correspond to the output signal of sensors that employ local piezoresistive elements for monitoring beam response (e.g., the piezoresistive Wheatstone bridge employed in [19]).

For each load case and each response history [$v(L,t)$ and $v_{B-D}(L,t)$], the following resonant characteristics will be determined: the resonant frequency f_{res}, defined as the exciting frequency corresponding to maximum displacement amplitude, and the

quality factor Q associated with viscous losses in the surrounding fluid. The primary emphasis of the study is on the fundamental (i.e., mode-1) in-plane flexural/shear response, although the theoretical solutions obtained may be used to generate multi-modal in-plane response. Once the resonant characteristics are determined, they may be related to sensor performance metrics, i.e., mass and chemical sensitivity (S_m, S_c) and limit of detection (LOD) (e.g., [20, 29-31]).

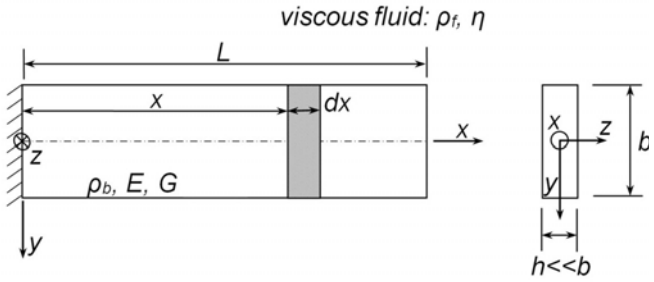

Figure 1: Definitions of reference axes and geometric and material parameters.

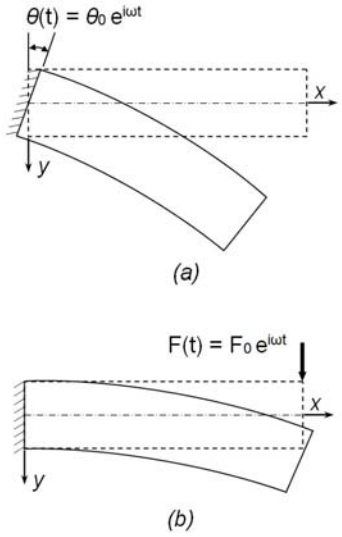

**Figure 2: (a) Load Case I – Imposed harmonic support rotation;
(b) Load Case II – Imposed harmonic tip force.**

III. DERIVATION OF BOUNDARY VALUE PROBLEM

A. Assumptions

The physical system comprising the microcantilever and surrounding fluid is idealized by employing the following assumptions: (1) The beam is homogeneous and made of a material that is linear elastic and isotropic. (2) The beam is of uniform, rectangular cross section. (3) The slope of the deformed beam centerline is much smaller than unity. (4) The beam support is rigid (support deformation is neglected). (5) The loading is harmonic and applied in-plane, resulting in only in-plane flexural/shear deformation. (6) The cross section is relatively thin, i.e., $h<<b$, so that the fluid resistance associated with the pressure on the top and bottom faces in Fig. 1 and the shear stress and pressure on the end face (at $x=L$) is negligible compared with that due to the fluid's shear resistance on the two largest faces. (7) The shear stress exerted by the fluid on the beam is modeled by local application of the solution of Stokes's second problem for harmonic, in-plane oscillations of an infinite rigid surface in contact with a viscous fluid ([38], e.g., [39]). (8) Viscous energy losses in the fluid are the dominant loss mechanism. The combination of assumptions 6 and 7 are referred to here as the assumption of "Stokes fluid resistance," which is a generalization to the case of Timoshenko beam theory of the assumption made in Heinrich et al. [17-18] for Euler-Bernoulli beam theory.

B. Derivation of Equations of Motion

The basis of Timoshenko beam theory is the decomposition of the total deflection into bending and shear contributions [40-41], i.e.,

$$v(x,t) = v_B(x,t) + v_S(x,t)\,, \tag{1}$$

where v_B is the deflection due to bending and v_S is the deflection due to shear. A similar decomposition of the slope of the deformed beam axis therefore results from Eq. (1):

$$\frac{\partial v}{\partial x} = \frac{\partial v_B}{\partial x} + \frac{\partial v_S}{\partial x} \equiv \varphi(x,t) + \psi(x,t), \tag{2}$$

in which φ represents the rotation of the beam cross section and ψ is the transverse shear strain.

The classical solution to Stokes's second problem [38] for the harmonic, in-plane, translational oscillation of an infinite, rigid surface in contact with a viscous fluid results in a simple form for the shear stress, $\tau_{fluid}(t)$,exerted by the fluid on the oscillating surface:

$$\tau_{fluid}(t) \equiv -\sqrt{\frac{\rho_f \eta}{2\omega}}\, \dot{V}_{surf.}(t) - \sqrt{\frac{\rho_f \eta \omega}{2}}\, V_{surf.}(t) \qquad , \tag{3}$$

where $V_{surf.}(t)$ and $\dot{V}_{surf.}(t)$ are the (harmonic) velocity and acceleration of the surface and ω is the frequency of oscillation. To apply Eq. (3) to the present problem, we assume that each cross section translates and rotates rigidly and that Eq. (3) may be applied pointwise on the slice *dx* of Fig. 1. This leads to a relatively simple, yet mechanics-based, fluid resistance model to provide a first attempt at understanding how the fluid properties influence the dynamic response of a micro-scale Timoshenko beam. More specifically, applying Eq. (3) locally at all points on the front and rear faces of the differential element of Fig. 1, followed by an appropriate integration over the *y*-coordinate, results in the following fluid-induced force and couple distributions (per unit length) along the beam [31]:

$$q_{fluid}(x,t) = -\overline{m}_f \frac{\partial^2 v(x,t)}{\partial t^2} - \overline{c}_f \frac{\partial v(x,t)}{\partial t}, \tag{4a}$$

$$c_{fluid}(x,t) = -\frac{\overline{m}_f b^2}{12}\frac{\partial^2 \varphi}{\partial t^2} - \frac{\overline{c}_f b^2}{12}\frac{\partial \varphi}{\partial t} \quad , \tag{4b}$$

where the coefficients in Eq. (4a),

$$\overline{m}_f \equiv \sqrt{\frac{2\rho_f \eta b^2}{\omega}} \ , \ \ \overline{c}_f = \sqrt{2\rho_f \eta b^2 \omega} \ , \tag{5a,b}$$

are, respectively, the effective translational fluid mass and fluid damping coefficients per unit length of beam. Similarly, the coefficients in Eq. (4b) may be interpreted as effective rotational fluid mass and fluid damping coefficients. Using the fluid-induced loads determined above, one may easily generalize the derivation of the in-vacuum equations of motion for a Timoshenko beam (e.g., [42]) by incorporating these loads into the translation and rotational dynamic equilibrium statements for the differential element, thus yielding the following equations of motion [31]:

$$\frac{\partial^2 \overline{v}}{\partial \xi^2} - \frac{\partial \varphi}{\partial \xi} - s^2 \lambda^3 \left(\lambda + \zeta\right) \frac{\partial^2 \overline{v}}{\partial \tau^2} - s^2 \lambda^3 \zeta \frac{\partial \overline{v}}{\partial \tau} = 0 \, , \tag{6a}$$

$$s^2 \frac{\partial^2 \varphi}{\partial \xi^2} + \frac{\partial \overline{v}}{\partial \xi} - \varphi - r^2 s^2 \lambda^3 \left(\lambda + \zeta\right) \frac{\partial^2 \varphi}{\partial \tau^2} - r^2 s^2 \lambda^3 \zeta \frac{\partial \varphi}{\partial \tau} = 0 \, , \tag{6b}$$

where $\overline{v} \equiv v / L$ is the dimensionless total deflection, $\xi \equiv x / L$ is a dimensionless spatial coordinate, and $\tau \equiv \omega t$ is dimensionless time. The "Timoshenko beam parameters" are defined as the rotational inertia parameter and the shear deformation parameter, respectively, via

$$r^2 \equiv \frac{I}{AL^2} = \frac{1}{12}\left(\frac{b}{L}\right)^2 \ , \tag{7a}$$

$$s^2 \equiv \frac{EI}{kAGL^2} = \frac{1}{12}\left(\frac{b}{L}\right)^2 \left(\frac{E}{kG}\right) \ , \tag{7b}$$

where A and I represent the cross-sectional area and the second moment of area of the rectangular cross section, the latter corresponding to in-plane bending ($I=hb^3/12$), and k

($\approx 5/6$) is the shear coefficient for a rectangular cross section [43]. The dimensionless frequency and fluid resistance parameters (λ and ζ, respectively) are defined by

$$\lambda \equiv \left(\frac{12\rho_b L^4 \omega^2}{Eb^2} \right)^{1/4} \quad , \quad \zeta \equiv \frac{L}{hb^{1/2}} \left(\frac{48\rho_f{}^2 \eta^2}{E\rho_b{}^3} \right)^{1/4} \quad . \tag{8a,b}$$

The fluid effects appear in Eqs. (6a,b) through those terms that involve ζ. When this parameter is set equal to zero, the equations reduce to the well-known in-vacuum results (e.g., [42, 44]).

C. Boundary Conditions

For each load case four boundary conditions (BCs) must be specified as follows:

Load Case I (Harmonic Support Rotation, Fig. 2a):

$$\overline{v}(0,\tau) = 0 \quad , \quad \varphi(0,\tau) = \theta_0 e^{i\tau} \quad , \quad \frac{\partial \varphi(1,\tau)}{\partial \xi} = \frac{\partial \overline{v}(1,\tau)}{\partial \xi} - \varphi(1,\tau) = 0 \quad ; \tag{9a-d}$$

Load Case II (Harmonic Tip Force, Fig. 2b):

$$\overline{v}(0,\tau) = \varphi(0,\tau) = \frac{\partial \varphi(1,\tau)}{\partial \xi} = 0 \quad , \quad \frac{\partial \overline{v}(1,\tau)}{\partial \xi} - \varphi(1,\tau) = s^2 \overline{F}_0 e^{i\tau} \quad ; \tag{10a-d}$$

where a dimensionless tip force amplitude has been introduced in Eq. (10d):

$$\overline{F}_0 \equiv F_0 L^2 / EI \quad . \tag{11}$$

For each load case the BCs correspond, respectively, to imposed values of deflection and rotation at the supported end and bending moment and shear force at the unsupported end.

The BVPs to be solved consist of the governing equations, Eqs. (6a,b), and the corresponding set of BCs: Eqs. (9a-d) for Load Case I or Eqs. (10a-d) for Load Case II.

D. Secondary Fields

Since the Timoshenko beam response is completely described using the "primary fields," $\bar{v}$ and φ, any additional "secondary" fields are derivable directly from $\bar{v}$ and φ once they have been determined. In particular, the time-dependent beam displacement due to bending is obtained by integrating the rotation angle:

$$\bar{v}_B(\xi,\tau) = \int_0^\xi \varphi(\xi',\tau)d\xi' \quad , \tag{12}$$

where $\bar{v}_B \equiv v_B / L$. For Load Case I a portion of $\bar{v}_B$ is due to rigid-body rotation associated with the end-rotation loading (Fig. 2a). Thus, the deflection due to bending *deformation* in the two load cases may be written as

$$\bar{v}_{B-D}(\xi,\tau) = \begin{cases} \displaystyle\int_0^\xi \varphi(\xi',\tau)d\xi' - \theta_0 \xi e^{i\tau} \quad , \text{ Load Case I;} \\ \displaystyle\int_0^\xi \varphi(\xi',\tau)d\xi' \quad , \text{ Load Case II.} \end{cases} \tag{13a,b}$$

The normalized shear displacement, if desired, may be obtained for either load case by substituting $\bar{v}(\xi,\tau)$ and Eq. (12) into Eq. (1):

$$\bar{v}_S(\xi,\tau) \equiv \frac{v_S(\xi,\tau)}{L} = \bar{v}(\xi,\tau) - \int_0^\xi \varphi(\xi',\tau)d\xi' \, . \tag{14}$$

IV. METHOD OF SOLUTION

The steady-state solution of the BVP for either load case is assumed to be of the form

$$\bar{v}(\xi,\tau) = \bar{V}(\xi)e^{i\tau} \quad , \qquad \varphi(\xi,\tau) = \Phi(\xi)e^{i\tau} \quad , \tag{15a,b}$$

where $\bar{V}(\xi)$ and $\Phi(\xi)$ are the complex amplitudes to be determined. It follows from Eqs. (6a,b) that $\bar{V}(\xi)$ and $\Phi(\xi)$ must satisfy

$$\bar{V}'' + k_3 \bar{V} - \Phi' = 0\,, \tag{16a}$$

$$s^2 \Phi'' + \bar{V}' - \left(1 - r^2 k_3\right)\Phi = 0\,, \tag{16b}$$

which may also be expressed in the following uncoupled form [32, 44]:

$$\bar{V}'''' + k_1 \bar{V}'' + k_2 \bar{V} = 0\,, \tag{17a}$$

$$\Phi'''' + k_1 \Phi'' + k_2 \Phi = 0\,, \tag{17b}$$

where

$$k_1 \equiv \lambda^3 \left(r^2 + s^2\right)\left[\lambda + \left(1 - i\right)\zeta\right], \tag{18a}$$

$$k_2 \equiv -\lambda^3 \left[\lambda + (1-i)\zeta\right]\left\{1 - r^2 s^2 \lambda^3 \left[\lambda + \left(1-i\right)\zeta\right]\right\}, \tag{18b}$$

$$k_3 \equiv s^2 \lambda^2 \left[\lambda\left(\lambda + \zeta\right) - i\lambda\zeta\right]\,, \tag{18c}$$

and the primes in Eqs. (16) and (17) indicate differentiation with respect to ξ. Next we determine the steady-state solution for each particular load case.

Load Case I: Harmonic Support Rotation

For Load Case I we write the general solutions of Eqs. (17a,b) as

$$\bar{V}(\xi) = \theta_0 \left[C_1 \cosh(n_1 \xi) + C_2 \sinh(n_1 \xi) + C_3 \cos(i n_2 \xi) + C_4 \sin(i n_2 \xi)\right], \tag{19a}$$

$$\Phi(\xi) = \theta_0 \left[C_1' \sinh(n_1 \xi) + C_2' \cosh(n_1 \xi) + C_3' \sin(i n_2 \xi) + C_4' \cos(i n_2 \xi)\right], \tag{19b}$$

where n_1 and n_2 are the two roots of

$$n^4 + k_1 n^2 + k_2 = 0 \tag{20}$$

that have positive real parts. By virtue of Eq. (16a) or (16b), the constants C_i and C_i', i=1, 2, 3, 4, are related by

$$C_{1,2}{}' = \frac{n_1^2 + k_3}{n_1} C_{1,2} \quad , \quad C_{3,4}{}' = \mp \frac{i\left(n_2^2 + k_3\right)}{n_2} C_{3,4} \quad . \qquad \text{(21a-d)}$$

Imposing the BCs (9a-d) yields the specific values of C_1 through C_4 as detailed in the Appendix. The values of these four constants, in conjunction with Eqs. (15a,b), (19a,b), and (21a-d), determine the steady-state solution for the case of harmonic support rotation.

Load Case II: Harmonic Tip Force

For Load Case II we write the general solutions of Eqs. (17a,b) as

$$\bar{V}(\xi) = \bar{F}_0 \left[C_1 \cosh(n_1 \xi) + C_2 \sinh(n_1 \xi) + C_3 \cos(i n_2 \xi) + C_4 \sin(i n_2 \xi) \right], \qquad \text{(22a)}$$

$$\Phi(\xi) = \bar{F}_0 \left[C_1{}' \sinh(n_1 \xi) + C_2{}' \cosh(n_1 \xi) + C_3{}' \sin(i n_2 \xi) + C_4{}' \cos(i n_2 \xi) \right], \qquad \text{(22b)}$$

where the constants, C_i , C_i' , will take on different values than in the previous load case. However, the definitions of n_1 and n_2 through Eq. (20) and the relationships between C_i and C_i' (Eqs. (21a-d)) are still applicable for Load Case II. Imposing the BCs (10a-d) for Load Case II yields the specific values of C_1 through C_4 as detailed in the Appendix. The values of these four constants, in conjunction with Eqs. (15a,b), (22a,b), and (21a-d), determine the steady-state solution for the case of a harmonic tip force.

V. RESULTS AND DISCUSSION

A. Normalized Response Quantities

Having obtained the solutions for the in-fluid Timoshenko beam response for the two load cases of interest, any secondary field of interest (e.g., displacements due to bending deformation or shear deformation) may be determined in the manner specified in Sect. III-D. In particular, as explained in Sect. II, since cantilever response is often detected using either optical techniques to track the beam tip position or piezoresistive elements to monitor bending strain, the magnitudes of both the total tip displacement amplitude and the bending–deformation displacement amplitude at the tip are of practical interest. Therefore, the numerical results to be presented in subsequent sections will be based on the following normalized response metrics associated with these two types of output signals (subscripts *T* and *B-D* denoting "total" and "bending-deformation," respectively):

$$D_T = \begin{cases} \left|\bar{V}(1)\right| / \theta_0 \quad , & \text{Load Case I ;} \\ 3\left|\bar{V}(1)\right| / \bar{F}_0 \quad , & \text{Load Case II ;} \end{cases} \tag{23a,b}$$

$$D_{B-D} = \begin{cases} \left| \dfrac{\int_0^1 \Phi(\xi')d\xi'}{\theta_0} - 1 \right| \quad , & \text{Load Case I ;} \\ \dfrac{3\left| \int_0^1 \Phi(\xi')d\xi' \right|}{\bar{F}_0} \quad , & \text{Load Case II.} \end{cases} \tag{24a,b}$$

These quantities may be interpreted as "dynamic magnification factors" in the following senses: D_T and D_{B-D} are, respectively, the magnitudes of the total tip displacement

amplitude (bending plus shear, including rigid-body rotation in Load Case I) and the bending-deformation tip displacement, each scaled by the corresponding quasi-static Euler-Bernoulli results (i.e., $L\theta_0$ for Load Case I and $F_0L^3/3EI$ for Load Case II). The analogous result for D_S, the normalized magnitude of the tip displacement amplitude due to shear deformation only (scaled in the same manner as D_T and D_{B-D}), is

$$D_S = \begin{cases} \dfrac{\left|\bar{V}(1) - \displaystyle\int_0^1 \Phi(\xi')d\xi'\right|}{\theta_0} & , \quad \text{Load Case I} \ ; \\ \dfrac{3\left|\bar{V}(1) - \displaystyle\int_0^1 \Phi(\xi')d\xi'\right|}{\bar{F}_0} & , \quad \text{Load Case II} \ . \end{cases} \tag{25a,b}$$

Finally, we emphasize that the analytical solution presented in the previous section may be used to obtain other relevant mechanical response quantities that correspond to other readout methods.

B. Theoretical Numerical Results

1. Frequency Response

The theoretical solutions obtained may be used to generate frequency response functions for the tip displacement amplitude for any output signal (D_T, D_{B-D}, or D_S) and for either load case (harmonic support rotation or tip force). While our main interest is to focus on resonant characteristics and not the entire frequency spectrum, for illustrative purposes we show some examples of the relevant frequency response

functions in Figs. 3a and 3b for Load Cases I and II, respectively. These figures correspond to fixed values of r=0.2 and ζ =0.2 while the value of the material parameter

$$e \equiv \sqrt{\frac{E}{kG}} \tag{26}$$

is allowed to vary. Note that an increase in e corresponds to a reduction in shear modulus relative to the Young's modulus, so that e may be viewed as a shear deformation parameter in lieu of parameter s. The plots indicate that an increase in e results in a decrease in the resonant frequency as measured by any of the signals. This is to be expected since the reduction in beam stiffness due to a lower shear stiffness will cause a corresponding reduction in resonant frequency since the mass characteristics remain unchanged for a fixed r value. These figures also show that an increase in e in the case of harmonic support rotation (Fig. 3a) causes a decrease in the resonant amplitude of the total tip displacement (D_T), while for the harmonic tip force case (Fig. 3b) the resonant amplitude increases with increasing e. However, if one considers the resonant amplitudes of the bending-deformation and shear portions of the tip displacement (D_{B-D} and D_S) as the value of e increases, one finds that the strength of the D_{B-D} signal at resonance decreases for both load cases, while the strength of the shear signal increases. Similar conclusions apply with respect to changes in the value of r , although the corresponding figures are not included here.

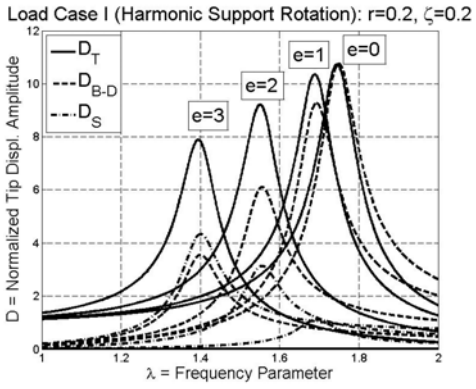

(a)

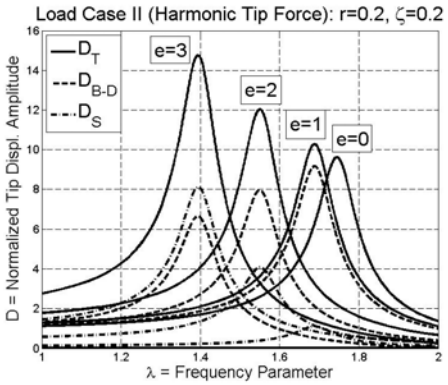

(b)

Figure 3: Theoretical frequency response functions for tip displacement amplitude: (a) Load Case I – Imposed harmonic support rotation; (b) Load Case II – Imposed harmonic tip force.

The different resonant amplitudes of the various output signals could have important implications with regard to the appropriate design of detection schemes for these types of sensing devices. For example, a detection scheme based on monitoring of bending strain (e.g., via piezoresistors at the extreme fibers of the beam) might only "see" a small portion of the deformation response if a significant amount of shear deformation is present. In such a case, one may wish to replace or supplement the bending-strain detection scheme with shear strain measurements near the neutral axis of the beam's cross section.

All of the numerical results that follow will focus on the resonant frequency and quality factor of lateral-mode mirocantilevers in liquids. Theoretical values of these resonant quantities may easily be extracted from frequency response curves of the type shown in Figs. 3a,b. In the present study our interest is in micro-scale devices in liquids whose properties are on the same order as that of water. As such, a practical range of the fluid resistance parameter for these types of applications is $0 \le \zeta \le 0.2$. (As a reference, a silicon device of dimensions (*L, b, h*)=(500, 200, 10) μm and operating in water corresponds to $\zeta = 0.043$. If water is changed to a hypothetical liquid of twice the density and 10 times the viscosity, then $\zeta = 0.19$.) Over this range the values of resonant frequency and quality factor are very insensitive to both the load case and the output signal employed [45]. Therefore, unless stated otherwise, all results that follow will be based on Load Case I (harmonic support rotation) and the total tip displacement signal. The analogous results for Load Case II and/or other output signals will be practically identical over the range of ζ considered. (For example, despite the significant differences in the amplitude spectra of Fig. 3 for the different load cases and detection signals, the peak locations, i.e., resonant frequencies, are very insensitive to the load/detection type, even at the upper limit of this range of ζ. Although less apparent, this same insensitivity is exhibited by the mode-1 quality factor for $\zeta \in [0, 0.2]$. Details may be found in [31]. The same reference includes results and discussion associated with higher values of the fluid resistance parameter.) However, at higher values of ζ, which may be encountered for more viscous and/or denser liquids or for nano-scale devices, the values of resonant frequency and quality factor will show increased sensitivity to load type and the response monitoring scheme; therefore, in such cases one should employ the

specific solution that applies to the particular methods of actuation and detection in the physical device [45].

2. Resonant Frequency

The resonant frequency parameter, λ_{res} , for the first lateral mode is plotted in Figs. 4a-d for the case of harmonic support rotation. These figures show the dependence of resonant frequency on the fluid resistance parameter, ζ, and the Timoshenko parameters, as characterized by parameters r and e. These resonant frequency values correspond to the first peaks of the frequency response functions for the total tip displacement (curves of the type labeled "D_T" in Fig. 3a).

Figure 4 clearly illustrates several trends. As expected, there is a reduction in resonant frequency associated with an increase in the fluid resistance parameter. Moreover, for the range of ζ considered the dependence of λ_{res} on ζ is essentially linear. This was also seen in the results of the previously published resonant frequencies of the Euler-Bernoulli model [18], which are a special case (r=e=0 or, equivalently, r=s=0) of the results shown here. Also observed in Fig. 4 is how higher levels of r and e values, corresponding to increased beam inertia and decreased shear stiffness, will result in a reduction in resonant frequency. Over the practical ranges of parameters considered in

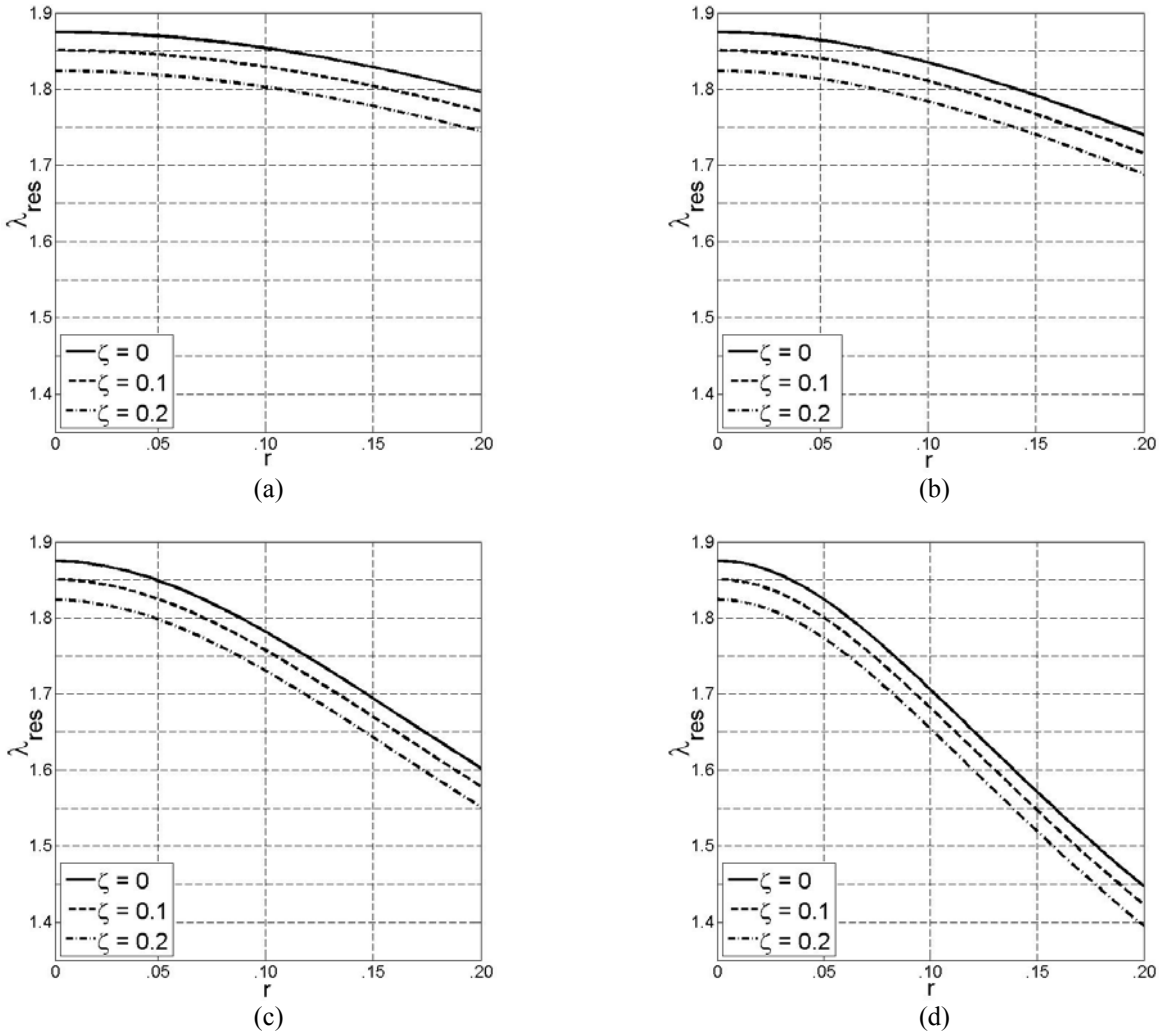

Figure 4: Resonant frequency based on D_T signal for Load Case I: (a) e=0, (b) e=1, (c) e=2, (d) e=3.

Fig. 4, the maximum effect of r and e is to cause a reduction of 23% in λ_{res} which, according to Eq. (8a), is equivalent to a decrease in the resonant frequency, ω_{res}, of 40%. These reductions correspond to the case of r=0.2, e=3. If we consider the case e=2, which corresponds to "textbook" values of moduli for silicon for the case in which the cantilever is aligned with the [110]-direction of a standard (100) Si wafer (E=169 GPa, G=50.9 GPa [46]) and shear coefficient k=5/6, Fig. 4c shows that the largest influence of the Timoshenko effects on the resonant frequency is a 15% (28%) decrease

in λ_{res} (ω_{res}), which occurs at r=0.2. Clearly, significant error may be introduced in the resonant frequency estimate if the Timoshenko effects are ignored in such cases. Conversely, calculations based on the results of Fig. 4 show that, over the practical ranges of ζ and e considered, the influence of the Timoshenko effects on resonant frequency (ω_{res}) is less than 2% provided that the ratio L/b is 10 or greater (or, equivalently, that r does not exceed 0.029). Finally, as a verification of the resonant frequency results, we find that the values in Figs. 4a-d for the case $r = \zeta = 0$ (i.e., the starting values of the four upper curves) are all given by λ_{res} = 1.8751, which agrees with the well-known eigenvalue for an Euler-Bernoulli beam in vacuum (e.g., [47]).

3. Quality Factor

Applying the -3dB bandwidth method (e.g., [48]) to the response curves of the type shown in Fig. 3, one may obtain the quality factor for a range of fluid resistance and Timoshenko parameters. For example, the quality factor based on the total tip displacement for the harmonic support rotation case is plotted in Fig. 5 over the range $\zeta \in [0, 0.2]$ for the case of r=0.13. Clearly, there is a very strong impact of ζ on Q with the quality factor following an inverse relationship with ζ. Recalling the definition of ζ [Eq. (8b)], the viscosity and density of the fluid participate to an equal extent in determining Q when a Stokes-type fluid resistance model is employed. Unlike the strong dependence of Q on ζ, the effect of increasing the Timoshenko parameter e from 0 to 3

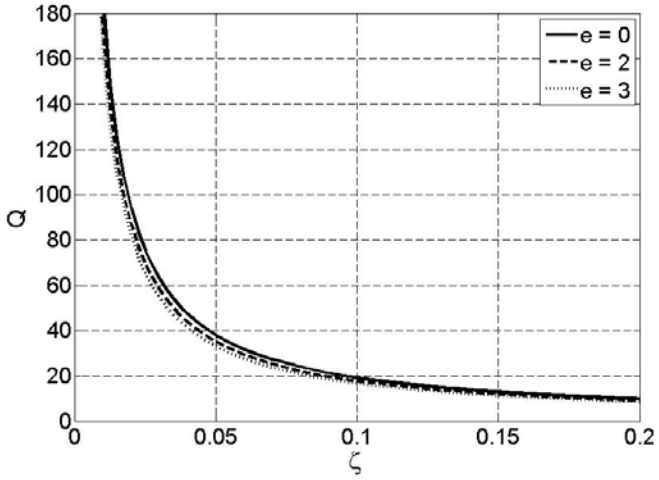

Figure 5: Quality factor at first resonance for r=0.13 (based on the D_T signal for Load Case I).

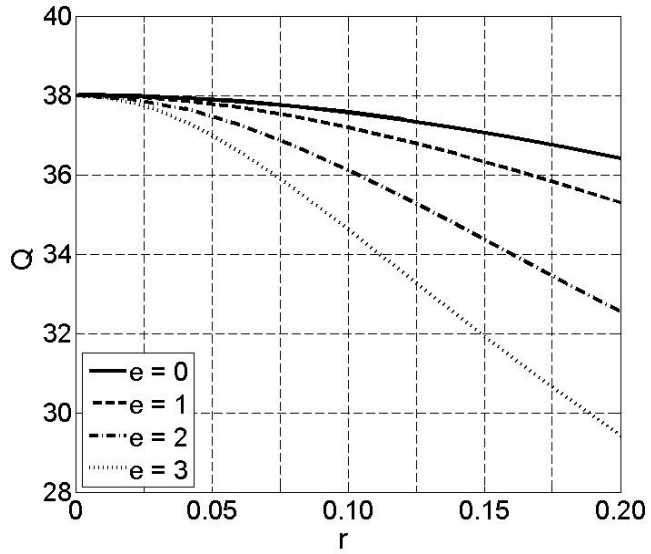

Figure 6: Quality factor at first resonance for ζ=0.05 (based on the D_T signal for Load Case I).

results in a relatively modest 15% reduction of the quality factor, even for the relatively large value of r considered. Similar trends apply for a specified value of e and varying r from 0 to 0.2, except the effects of changing r over this range are of even lesser magnitude than the effects of varying e.

Figure 6 contains the same type of information displayed in Fig. 5, but this information is plotted vs. the Timoshenko parameter r so its effect on Q may be ascertained. Again, the effects of the fluid resistance parameter on the quality factor are seen to be significant. The curves shown in Fig.6 show negligible sensitivity of Q to changes in r at small values of r , but this sensitivity increases with increasing r values, especially for larger values of e. This indicates that the effects of r on Q become increasingly significant for larger values of both r and e. Figure 6 also reinforces the earlier commentary that the Timoshenko effects, as characterized by r and e, cause a reduction in Q, as do the fluid effects associated with increases in ζ. Over the practical ranges of $0<\zeta<0.2$ and Timoshenko parameters considered in Fig. 6, the results of the present model show that the maximum effect of r and e on Q is to cause a reduction of approximately 23% regardless of the particular value of ζ. On the other hand, calculations based on the results such as those of Fig. 6 show that, over the practical ranges of ζ and e considered, the influence of the Timoshenko effects on Q is less than 1% provided that the ratio L/b is at least 10 (i.e., r does not exceed 0.029).

Previous theoretical investigations of lateral-mode Euler-Bernoulli beams with Stokes-type fluid resistance [17-18] have established an approximate analytical expression for Q. That expression indicated that Q is of the form $Q \approx 1.8751/\zeta$, i.e., Q depends inversely on ζ as was also surmised by a visual examination of the results of the present Timoshenko beam model in Fig. 5. Given that the dependence of Q on the Timoshenko parameters appears to be relatively simple as suggested by Figs. 5 and 6, we are motivated to pursue an approximate analytical formula for Q that will maintain the same ζ –dependence as the Euler-Bernoulli result while incorporating the r- and e-

dependence in a simple manner. Here we propose such an expression for the following ranges of parameters, which have been chosen based on micro-scale devices and common fluid properties: ζ = [0.01, 0.05], r = [0, 0.2] and $e \equiv \sqrt{E/kG}$ =[0, 3]. The expression is based on surface-fitting the results of the present model over the stated rectangle of the (r, e)-plane and maintaining the inverse relationship to ζ, thus yielding

$$Q \approx \frac{1.8751 - 3.427 r^{2.529} - 0.8267 r^{1.578} e^{1.646}}{\zeta} \quad , \tag{27a}$$

or, in terms of the fundamental system parameters (taking k=5/6),

$$Q \approx 0.7124 \frac{h b^{1/2}}{L} \left(\frac{E \rho_b^3}{\rho_f^2 \eta^2} \right)^{1/4} \left[1 - 0.0789 \left(\frac{b}{L} \right)^{2.529} - 0.0721 \left(\frac{b}{L} \right)^{1.578} \left(\frac{E}{G} \right)^{0.823} \right]. \tag{27b}$$

While the constants in Eqs. (27a,b) were based on fitting the model's results for the case of ζ = 0.03, the accuracy of these equations relative to the model's results over the practical range ζ = [0.01, 0.05] (and possibly beyond) is excellent (within 3%).

C. Comparisons between Theory and Experiment

1. Specification of Model Input Parameters

Experimental data were collected on a variety of silicon specimens excited laterally in water (ρ_f = 1000 kg/m^3, η = 0.001 Pa-s). The specimen geometries corresponded to nominal silicon thicknesses of h_{nom} = (5, 8, 12, 20) μm and length and width dimensions of L = (200, 400, 600, 800, 1000) μm and b = (45, 60, 75, 90) μm. Estimates of the total thickness (h), which includes the thicknesses of silicon and several passivation layers [21] was used as model input in lieu of h_{nom} and are listed in Table 1. To generate theoretical results it is also necessary to specify values of the material parameters $\bar{e} \equiv \sqrt{E/12\rho_b}$ and $e \equiv \sqrt{E/kG}$, which may be interpreted as parameters

associated with bending and shear deformation, respectively. However, the aforementioned multi-layer structure of the cantilevers makes it difficult to specify *a priori* the values of the effective moduli, E and G, and, thus, $\bar{e}$ and e. Therefore, two methods of specifying these parameters were explored.

In Method 1 the value of $\bar{e}$ was determined by performing a single-parameter fit of the in-vacuum resonant frequencies predicted by the model to in-air resonant frequency data, resulting in a value of $\bar{e}$=2.254 km/s which, using the density of silicon (2330 kg/m^3), corresponds to an effective E of 142 GPa. This fit was performed only on the data corresponding to specimen lengths L = (800, 1000) μm in order to avoid inclusion of additional effects associated with the shorter, "stubbier" specimens (i.e., Timoshenko beam effects and support compliance effects) in determining what is essentially a flexural stiffness parameter. Having determined $\bar{e}$ in this manner, the accompanying e (and G) value was then obtained by performing a second single-parameter fit of the in-air frequency data (with fitting parameter e) for each thickness set but for *all* specimen lengths; thus, any observed softening due to shear deformation will be reflected in the value of the material parameter e. This methodology resulted in the values of $\bar{e}$ and e (and E and G) listed under "Method 1" in Table 1. Using these as input, comparisons could then be made between in-water data and the predictions of the present model for both resonant frequency and quality factor. Sample comparisons for the thinnest specimen set (h_{nom}=5 μm) are shown in Fig. 7. While these results, based on Method 1 for prescribing input values, capture the f_{res} and Q trends quite well both

Table 1: Material parameters $\bar{e}$ and e and effective elastic moduli for each specimen thickness set, obtained by (a) Method 1 and (b) Method 2.

		(a) Method 1 (e based on fitting in-air frequency data)				(b) Method 2 (e based on properties of pure Si)			
h_{nom} (μm)	h (μm)	$\bar{e}$ (km/s)	e	E (GPa)	G (GPa)	$\bar{e}$ (km/s)	e	E (GPa)	G (GPa)
5	7.02	2.254	4.129	142	10.0	2.254	2	142	42.6
8	10.32	2.254	3.761	142	12.1	2.254	2	142	42.6
12	14.48	2.254	3.378	142	14.9	2.254	2	142	42.6
20	22.34	2.254	3.512	142	13.8	2.254	2	142	42.6

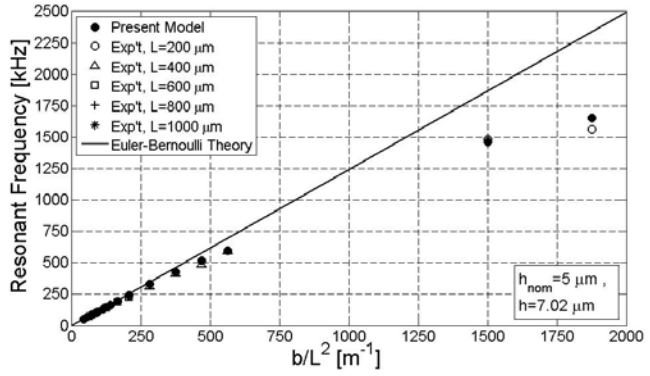

(a)

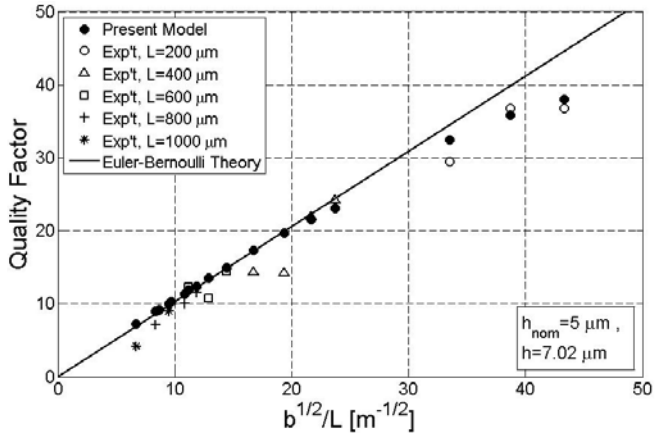

(b)

Figure 7: Comparison of present model (with Method 1-based input values of E=142 GPa, G=10.0 GPa) to experimental data in water [49] and Euler-Bernoulli theory [17-18] for h_{nom}=5 μm: (a) resonant frequencies and (b) quality factors for first lateral flexural mode.

qualitatively and quantitatively, examination of the G values that were used as input (column (a) of Table 1) shows that they are much lower (only 7-10% of E) than what would be expected for a multi-layer structure that is primarily silicon, for which G/E=0.30 for our case of cantilevers aligned with the [110]-direction of a (100) wafer [46]. A possible reason for this discrepancy could be that the G values based on Method 1 are artificially low to account indirectly for support compliance effects [50] that are not included in the present model. Therefore, to avoid such "overfitting" to account for non-Timoshenko beam effects, a second approach ("Method 2") was deemed to be a more rational method for specifying material input parameters to the model and was employed to generate all of the remaining numerical results in what follows.

Method 2 utilized the same methodology as Method 1 for determining the effective value of E=142 GPa, but prescribed the value of e (and thus G) to be consistent with the previously mentioned ratio of G/E=0.3 for single-crystal silicon. Thus, all theoretical results that follow will be based on the Method-2 input value of $e=\sqrt{(E/G)/k}=\sqrt{(1/0.3)/(5/6)}=2$, i.e., an effective shear modulus of $G=E/(ke^2)=142/[(5/6)(2)^2]$=42.6 GPa. (See column (b) of Table 1.)

2. Comparisons for Lateral-Mode Resonant Frequency and Quality Factor in Water: Model Predictions vs. Experimental Data

One of the primary motivations for the present study was the softening behavior exhibited by experimental data for lateral-mode resonant frequency and Q as microcantilevers become less slender. (E.g., see the departure from linearity of the data of Fig. 7 for the higher-Q specimens.) In what follows we therefore compare the results of the new model, using the Method-2 input parameters of Table 1, with experimental data

to ascertain the degree to which Timoshenko beam effects may account for the observed softening trends.

Theoretical in-water resonant frequency predictions using the present model are compared with experimental data in Fig. 8. The model yields frequency results that show the same qualitative softening trend as the data for larger b/L^2 values. However, of particular note is that the use of a more realistic G value in the model shows that the magnitude of the decrease in frequency for the stubbier beams cannot be explained solely by Timoshenko beam effects (shear deformation and rotatory inertia). A visual comparison of Figs. 8a-d indicates that the Timoshenko effects only account for roughly one-third of the frequency decrease relative to the Euler-Bernoulli model. Moreover, this observation seems to be independent of the specimen thickness. From a quantitative perspective, the current model overestimates the experimental frequency by 20-30% for the stubbiest specimens. This discrepancy is most likely due to support compliance effects and, in the case of the thicker specimens, the breakdown of the Stokes fluid resistance assumption (i.e., the neglected fluid pressure acting on the leading and trailing faces of the beam becomes significant for the thicker beams).

The theoretical in-water Q values predicted by the present model (applying the -3dB bandwidth method to the theoretical frequency response curves) are compared to experimental results and Euler-Bernoulli theory in Fig. 9, leading to the following observations: (1) while the current theoretical Q values consistently overestimate the experimental Q data, they provide a tighter upper bound than the previous Euler-

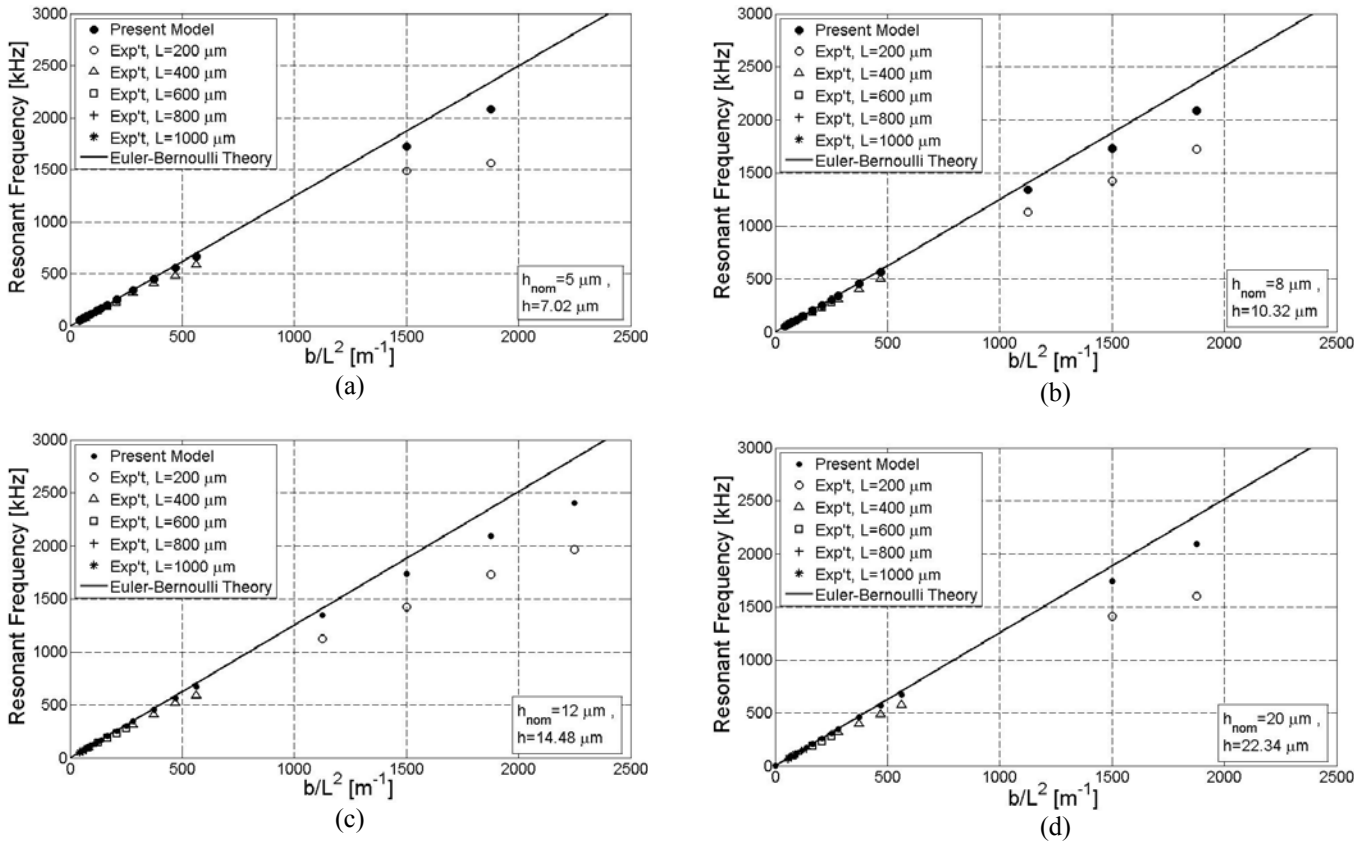

Figure 8: Comparison of present model (with Method 2-based input values of *E*=142 GPa, *G*=42.6 GPa) to experimental data [49] and Euler-Bernoulli theory [17] for in-water resonant frequencies of first lateral mode and for nominal thicknesses of (a) 5 μm (b) 8 μm (c) 12 μm and (d) 20 μm.

Bernoulli model (i.e., than the approximate analytical formula of [17-18]) for the less slender (higher *b/L*) specimens; (2) the theoretical *Q* based on the present model provides an excellent quantitative estimate for the thinner experimental specimen sets (i.e., nominal thicknesses of 5 μm and 8 μm), while for the thicker specimens the accuracy deteriorates due to the limitations (ignored pressure effects) of the Stokes-type fluid resistance assumption and potential support compliance effects; and (3) the theoretical *Q* predictions of the present model capture qualitatively the experimentally observed departure from linearity in *Q* (with respect to $b^{1/2}/L$) at higher values of $b^{1/2}/L$. Also of note is that the departure from linearity (i.e., from the Euler-Bernoulli results) is less

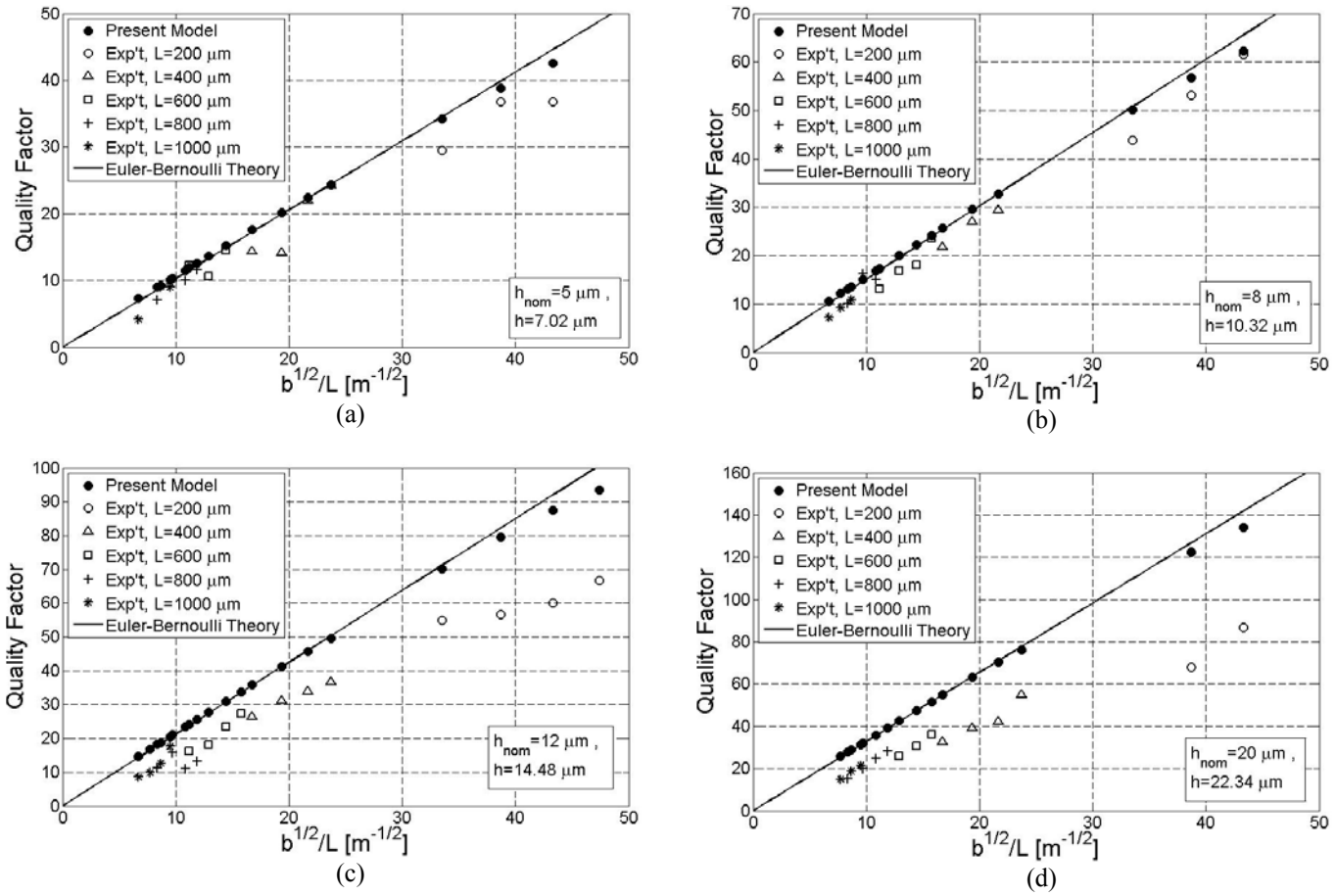

Figure 9: Comparison of present model (*E*=142 GPa, *G*=42.6 GPa) to experimental data [49] and Euler-Bernoulli theory [17] for in-water quality factor of first lateral mode and for nominal thicknesses of (a) 5 μm (b) 8 μm (c) 12 μm and (d) 20 μm.

pronounced for Q than for f_{res}. (Compare Figs. 8 and 9.) This may be explained by reference to fundamental vibration theory from which it is well known that for a single-degree-of-freedom system with effective stiffness K and effective mass M, the resonant frequency and quality factor are proportional to $\sqrt{K/M}$ and $\sqrt{KM}$, respectively. Thus, since the Timoshenko effects tend to decrease K and increase M, their effect on f_{res} will be more significant than on Q. This is predicted by the present model and reflected in the experimental data.

VI. SUMMARY AND CONCLUSIONS

A new analytical model has been developed for predicting the resonant characteristics of a Timoshenko cantilever beam in the presence of a viscous fluid. Since lateral-mode liquid-phase sensing applications provided the motivation for this study, an approximate, mechanics-based model for the fluid-resistance, based on Stokes's classical solution for in-plane oscillations, was introduced as a first attempt to rationally relate the inertial and damping effects of the fluid acting on the Timoshenko beam to the fluid's density and viscosity. The new model, which may be applied to multiple types of actuation and detection schemes, shows that the Timoshenko effects of shear deformation and rotatory inertia become quite important for lateral-mode cantilevers of small slenderness ratios, i.e., for those types of devices that have demonstrated higher quality factors (approaching 100) in liquids. Over the practical ranges of system parameters considered, the mode-1 results indicate that the Timoshenko effects can account for a reduction in f_{res} and Q of up to 40% and 23%, respectively, but are negligible (no more than a 2% reduction in f_{res} and a 1% reduction in Q) for length-to-width ratios of 10 and higher. Comparisons with experimental data in water indicate that the new model predicts qualitative trends in the data at higher b/L ratios and gives good quantitative estimates for Q for the thinner specimens considered. However, in other cases the model is seen to underestimate the softening trends in f_{res} and Q . This discrepancy is likely attributable to support deformation, thus providing motivation for future modeling efforts that account for support compliance in addition to the Timoshenko beam effects. Also, a generalization of the Stokes fluid resistance model to account for fluid pressure effects in future work is expected to improve the Q predictions for the case of thicker beams.

Acknowledgments

This work was supported in part by NSF Grant Nos. ECCS-0824017, ECCS-1128992, and ECCS-1128554 and the Graduate School of Marquette University.

References

[1] J.E. Sader, *J. Appl. Phys.* **84**, 64 (1998).
[2] S. Basak, A. Raman, and S.V. Garimella, *J. Appl. Phys.* **99**, 114906 (2006).
[3] C. Vančura, Y. Li, J. Lichtenberg, K.-U. Kirstein, A. Hierlemann, and F. Josse, *Anal. Chem.* **79**, 1646 (2007).
[4] C. Vančura, I. Dufour, S.M. Heinrich, F. Josse, and A. Hierlemann, *Sens. Act. A: Phys.* **141**, 43 (2008).
[5] T. Braun, V. Barwich, M.K. Ghatkesar, A.H. Bredekamp, C. Gerber, M. Hegner, and H.P. Lang, *Phys. Rev. E* **72**, 031907 (2005).
[6] C.A. Van Eysden and J.E. Sader, *J. Appl. Phys.* **101**, 044908 (2007).
[7] M.K. Ghatkesar, T. Braun, V. Barwich, J.-P. Ramseyer, C. Gerber, M. Hegner, and H.P. Lang, *Appl. Phys. Lett.* **92**, 043106 (2008).
[8] B.N. Johnson and R. Mutharasan, *J. Appl. Phys.* ***109***, 066105 (2011).
[9] C. Castille, I. Dufour, and C. Lucat, *Appl. Phys. Lett.* **96**, 154102 (2010).
[10] I. Dufour, F. Josse, S.M. Heinrich, C. Lucat, C. Ayela, F. Ménil, and O. Brand, *Sens. Act. B: Chem.* **170**, 115 (2012).
[11] R. Lakhmi, H. Debeda, I. Dufour, C. Lucat, and M. Maglione, *Int'l J. Appl. Ceramics Tech.* **11**, 311 (2014).
[12] C.P. Green and J.E. Sader, *J. Appl. Phys.* **92**, 6262 (2002).
[13] L.B. Sharos, A. Raman, S. Crittenden, and R. Reifenberger, *Appl. Phys. Letters* **84**, 4638 (2004).
[14] T. Cai, F. Josse, S. Heinrich, N. Nigro, I. Dufour, and O. Brand, *Proc., IEEE Int'l Freq. Control Symp. 2012*, Paper 7175, 6 pp. (2012).
[15] M. Aureli, C. Pagano, and M. Porfiri, *J. Appl. Phys.* **111**, 124915 (2012).
[16] I. Dufour, S.M. Heinrich, and F. Josse, *JMEMS* **16**, 44 (2007).
[17] S.M. Heinrich, R. Maharjan, L. Beardslee, O. Brand, I. Dufour, and F. Josse, *Proc., Int'l Workshop on Nanomechanical Cantilever Sensors*, Banff, Canada, 2 pp. (2010).
[18] S. Heinrich, R. Maharjan, I. Dufour, F. Josse, L.A. Beardslee, and O. Brand, *Proc., IEEE Sensors 2010 Conf.*, Waikoloa, HI, 1399 (2010).
[19] L.A. Beardslee, A.M. Addous, S.Heinrich, F. Josse, I. Dufour, and O. Brand, *JMEMS* **19**, 1015 (2010).
[20] L.A. Beardslee, K.S. Demirci, Y. Luzinova, B. Mizaikoff, S.M. Heinrich, F. Josse, and O. Brand, *Anal. Chem.* **82**, 7542 (2010).
[21] L.A. Beardslee, F. Josse, S.M. Heinrich, I. Dufour, and O. Brand, *Sens. Act. B: Chem.* **164**, 7 (2012).
[22] R. Cox, F. Josse, F., S.M. Heinrich, S., O. Brand, and I. Dufour, *J. Appl. Phys.* **111**, 014907 (2012).
[23] J.H. Seo and O. Brand, *JMEMS* **17**, 483 (2008).
[24] A. Rahafrooz and S. Pourkamali, *Proc., IEEE Sensors Conf.*, 1071 (2010).

[25] A. Rahafrooz and S. Pourkamali, *Proc., IEEE Int'l Freq. Control Symp. 2011*, 5 pp. (2011).
[26] M.S. Sotoudegan, S.M. Heinrich, F. Josse, N.J. Nigro, I. Dufour, and O. Brand, *Proc., 2013 Nanomechanical Sensing Workshop (NMC 2013)*, Stanford, CA,107 (2013).
[27] M.S. Sotoudegan, S.M. Heinrich, F. Josse, N.J. Nigro, I. Dufour, and O. Brand, *Proc., IEEE Sensors 2013 Conf.*, Baltimore, MD, 1164 (2013).
[28] M.S. Sotoudegan, S.M. Heinrich, F. Josse, I. Dufour, and O. Brand, *Proc., 2014 Nanomechanical Sensing Workshop (NMC 2014)*, Madrid, Spain, 2 pp. (2014).
[29] I. Dufour, F. Lochon, S.M. Heinrich, F. Josse, and D. Rebière, *IEEE Sensors Journal* **7**, 230 (2007b).
[30] R. Cox, F. Josse, M.J. Wenzel, S.M. Heinrich, and I. Dufour, *Anal. Chem.* **80**, 5760 (2008).
[31] J.A. Schultz, "Lateral-Mode Vibration of Microcantilever-Based Sensors in Viscous Fluids Using Timoshenko Beam Theory," *Ph.D. Dissertation*, Marquette University, Mlwaukee, WI (2012).
[32] J.-C. Hsu, H.-L. Lee, and W.-J. Chang, *Nanotechnology* **18**, 285503 (2007).
[33] M.H. Mahdavi, A. Farshidianfar, M. Tahani, S. Mahdavi, and H. Dalir, *Ultramicroscopy* **109**, 54 (2008).
[34] H.-L. Lee and W.-J. Chang, *Japanese Journal of Applied Physics* **48**, 065005 (2009).
[35] T.-L. Horng, *Proc., Int'l Conf. on Consumer Electronics, Communications and Networks (CECNet),IEEE*, Xianning, China, 3831 (2011).
[36] S. Abbasion, A. Rafsanjani, R. Avazmohammadi, and A. Farshidianfar, *Appl. Phys. Letters* **95**, 143122 (2009).
[37] Q. He and C.M. Lilley, *J. Appl. Phys.* **112**, 074322 (2012).
[38] G.G. Stokes, *Trans. Camb. Phil. Soc.* **9**, 8 (1851).
[39] F. White, *Viscous Fluid Flow*, 3rd ed., McGraw-Hill (2006).
[40] S.P. Timoshenko, *Phil. Mag.* **41**, 744 (1921).
[41] S.P. Timoshenko, *Phil. Mag.* **43**, 125 (1922).
[42] S. Timoshenko and D.H. Young, *Vibration Problems in Engineering*, Third Edition, Van Nostrand, New York (1955).
[43] G.R. Cowper, *J. Appl. Mech.*. **33**, 335 (1966).
[44] T.C. Huang, *J. Appl. Mech.* **28**, 579 (1961).
[45] J.A. Schultz, J., S.M. Heinrich, F. Josse, I. Dufour, N.J. Nigro, L.A. Beardslee, and O. Brand, *Proc., 14th International Symposium on MEMS and Nanotechnology, SEM 2013 Annual Conference & Exposition on Experimental and Applied Mechanics,* Lombard, IL, Paper 155, 10 pp. (2013).
[46] M.A. Hopcroft, W.D. Nix, and T.W. Kenny, *JMEMS* **19**, 229 (2010).
[47] R.W. Clough and J. Penzien, *Dynamics of Structures*, Second Edition, McGraw-Hill, New York (1993).
[48] J.H. Ginsberg, *Mechanical and Structural Vibrations*, John Wiley and Sons, Inc., New York (2001).
[49] L.A. Beardslee, K.S. Demirci, Y. Luzinova, J.J. Su, B. Mizaikoff, S. Heinrich, F. Josse, and O. Brand, *Proc., Hilton Head Workshop 2010: A Solid-State Sensors, Actuators and Microsystems Workshop*, Hilton Head, SC, 4 pp. (2010).
[50] R. Maharjan, "Effect of Support Compliance on the Resonant Behavior of Microcantilever-Based Sensors in Viscous Fluids," *Ph.D. Dissertatio*n, Marquette University, Milwaukee, WI (2013).

APPENDIX: DETERMINATION OF CONSTANTS C_i , i=1, 2, 3, 4

The coefficients C_1, C_2, C_3, C_4 are obtained by solving the following system of linear algebraic equations:

$$[B]\{C\} = \{F\} \quad , \tag{A-1}$$

in which $\{C\} = \{C_1\ C_2\ C_3\ C_4\}^T$,

$$[B] = \begin{bmatrix} 1 & 0 & 1 & 0 \\ 0 & \dfrac{n_1^2 + k_3}{n_1} & 0 & \dfrac{i\left(n_2^2 + k_3\right)}{n_2} \\ \left(n_1^2 + k_3\right)\cosh n_1 & \left(n_1^2 + k_3\right)\sinh n_1 & \left(n_2^2 + k_3\right)\cos in_2 & \left(n_2^2 + k_3\right)\sin in_2 \\ -\dfrac{k_3 \sinh n_1}{n_1} & -\dfrac{k_3 \cosh n_1}{n_1} & \dfrac{ik_3 \sin in_2}{n_2} & -\dfrac{ik_3 \cos in_2}{n_2} \end{bmatrix} , \tag{A-2}$$

and

$$\{F\}^T = \begin{bmatrix} \{0 \quad 1 \quad 0 \quad 0\} & \text{for Load Case I;} \\ \{0 \quad 0 \quad 0 \quad s^2\} & \text{for Load Case II.} \end{bmatrix} \tag{A-3a,b}$$

Joshua A. Schultz graduated with his B.S. in Architectural Engineering and M.S. in Structural Engineering from the Milwaukee School of Engineering (MSOE) in 2009. He completed his Ph.D. in Civil Engineering at Marquette University in 2013 and became an Applied Research Engineer at Skidmore Owings and Merrill (SOM) in Chicago. Currently Dr. Schultz is Adjunct Professor and Director of Science, Technology, Engineering and Mathematics at MSOE. Dr. Schultz's research interests include multi-scale structural dynamics (ranging from MEMS to super-tall buildings), mechanics of composites and structural optimization.

Stephen M. Heinrich earned his B.S. degree *summa cum laude* from Penn State in 1980 and his M.S. and Ph.D. degrees from the University of Illinois at Urbana-Champaign in 1982 and 1985, all in civil engineering. He then joined the faculty at Marquette University as an Assistant Professor, being promoted in 1998 to his current rank of Professor of Civil Engineering. In 2000 Prof. Heinrich was awarded the *Reverend John P. Raynor Faculty Award for Teaching Excellence*, Marquette's highest teaching honor. Dr. Heinrich's research has focused on structural mechanics applications in microelectronics packaging and new analytical models for predicting and optimizing the performance of cantilever-based chemical/biosensors and, more recently, vibration energy harvesting devices. The investigations performed by Dr. Heinrich and his colleagues have resulted in over 100 refereed publications and three best paper awards from IEEE and ASME.

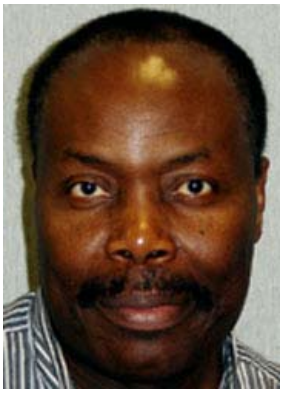

Fabien Josse received the License de Mathematics et Physique in 1976, the M.S. and Ph.D. degrees in Electrical Engineering from the University of Maine in 1979 and 1982, respectively. He has been with Marquette University, Milwaukee, WI, since 1982 and is currently professor in the Department of Electrical and Computer Engineering and in the Department of Biomedical Engineering. His research interests include solid state sensors, acoustic wave sensors and MEMS devices for liquid-phase biochemical sensor applications, investigation of novel sensor platforms, and smart sensor systems. Prof. Josse is a senior member of IEEE.

Isabelle Dufour graduated from Ecole Normale Supérieure de Cachan in 1990 and received the Ph.D. and H.D.R. degrees in engineering science from the University of Paris-Sud, Orsay, France, in 1993 and 2000, respectively. She was a CNRS research fellow from 1994 to 2007, first in Cachan working on the modeling of electrostatic actuators (micromotors, micropumps) and then after 2000 in Bordeaux working on microcantilever-based chemical sensors. She is currently Professor of electrical engineering at the University of Bordeaux and her research interests are in the areas of microcantilever-based sensors for chemical detection, rheological measurements and material characterization.

Nicholas J. Nigro (1934-2013) graduated with the B.S. from Michigan Technology University in 1956 and the M.S. from Iowa State University in 1959, both degrees being in civil engineering. Following a three-year period as an Instructor at Southern Illinois University, he pursued the Ph.D. in theoretical and applied mechanics at the University of Iowa, earning the doctoral degree in 1965. Subsequently, Dr. Nigro immediately began a distinguished 48-year career at Marquette University, during which time he directed the research of over 80 master's and Ph.D. students and was honored with six teaching awards, including the *Marquette University Teaching Excellence Award* in 1982. For the past six years Dr. Nigro served as a highly valued researcher as Professor Emeritus of Mechanical Engineering, interacting with students and faculty across the entire MU College of Engineering. Dr. Nigro's research portfolio spanned a diverse group of disciplines, including wave propagation, fluid-solid interaction, dynamics of high-altitude balloon systems, joining technology in electronic packaging, mechanics of liquid menisci, and, most recently, the modeling of MEMS resonators. Since his unexpected passing in December 2013, Dr. Nigro has been sadly missed by the large community of family, friends, colleagues, and students whose lives he enriched.

Luke A. Beardslee received a B.S. and Master of Engineering in Electrical Engineering from Cornell University in January 2007 and May 2007, and a Ph.D. in Electrical Engineering from the Georgia Institute of Technology in 2011. He is currently pursuing an M.D. degree at Albany Medical College in Albany, NY. His research interests include the application of micro/nanotechnology to biomedical and environmental problems, in particular biochemical sensors, implantable devices, and micromachined tissue engineering scaffolds.

Oliver Brand is a Professor in the School of Electrical and Computer Engineering and the Executive Director of the Institute for Electronics and Nanotechnology (IEN) at the Georgia Institute of Technology. He received his diploma degree in Physics from Technical University Karlsruhe, Germany in 1990 and his Ph.D. degree from ETH Zurich, Switzerland in 1994. From 1995 to 1997, he worked as a postdoctoral fellow at the Georgia Institute of Technology. From 1997 to 2002, he was a lecturer at ETH Zurich in Zurich, Switzerland and deputy director of the Physical Electronics Laboratory (PEL).

Dr. Brand has co-authored more than 190 publications in scientific journals and conference proceedings. He is a co-editor of the Wiley-VCH book series *Advanced Micro and Nanosystems* and a member of the editorial board of *Sensors and Materials*. He has served as General Co-Chair of the *2008 IEEE International Conference on Micro Electro Mechanical Systems (MEMS 2008)* and been a member of technical program committees of the *IEEE MEMS Conference*, the *IEEE Sensors Conference* and the *Transducers Conference*. Dr. Brand is a senior member of the *IEEE* and a co-recipient the *2005 IEEE Donald G. Fink Prize Paper Award*. His research interests are in the areas of integrated microsystems, microsensors, MEMS fabrication technologies, and microsystem packaging.